JOURNAL OF Applied Polymer SCIENCE

Nonisothermal Crystallization Behaviors of Poly(3-Hexylthiophene)/ Reduced Graphene Oxide Nanocomposites

Ziping Yang,[1,2] Hongbin Lu[1,2]

[1]State Key Laboratory of Molecular Engineering of Polymers, Fudan University, Shanghai 200433, China
[2]Department of Macromolecular Science, Fudan University, Shanghai 200433, China
Correspondence to: H. Lu (E-mail: hongbinlu@fudan.edu.cn)

ABSTRACT: Poly(3-hexylthiophene) (P3HT)/reduced graphene oxide (rGO) nanocomposites were prepared through *in situ* reduction of graphene oxide in the presence of P3HT. The nonisothermal crystallization behaviors of P3HT and P3HT/rGO nanocomposites were investigated by differential scanning calorimetry. The Avrami, Ozawa, and Mo models were used to analyze the nonisothermal kinetics. The addition of rGO remarkably increased the crystallization peak temperature and crystallinity of P3HT, but the crystallization half-time revealed little variation. The crystallization activation energies were calculated by the Kissinger equation. The results suggested that rGO plays a twofold role in the nonisothermal crystallization of P3HT, that is, rGO promotes the crystallization of P3HT as nucleating agent, and meanwhile, it also restricts the motion of P3HT chains. © 2012 Wiley Periodicals, Inc. J. Appl. Polym. Sci. 000: 000–000, 2012

KEYWORDS: poly(3-hexylthiophene); reduced graphene oxide; nonisothermal crystallization kinetics; nanocomposites

Received 29 February 2012; accepted 25 June 2012; published online
DOI: 10.1002/app.38265

INTRODUCTION

Poly(3-hexylthiophene) (P3HT) is one of the most extensively studied conjugate polymers for applications in plastic electronics including organic photovoltaics and field effect transistors.[1,2] The performance of devices depends largely on the structure and morphology of polythiophene in the active layer. As a result, it has been the subject of numerous studies how to control the morphology, crystal structure, and crystallization behavior of polythiophene, especially the effect of the electron acceptors, for example, fullerene, on the crystallization behavior of P3HT.[3–11]

With its excellent mechanical, electronic, and thermal properties, graphene has recently become a shining star in materials science.[12] Our and other studies have demonstrated that adding a small amount of graphene sheets into polymer matrices is sufficient to significantly improve the electrical, thermal, and mechanical properties of the resulting composites.[13–16] Recently, Chen and coworkers[17,18] suggested that graphene was able to act as a novel electron-accepting material in photovoltaics. Liu and coworkers[19] prepared P3HT/graphene nanocomposites via *in situ* reduction of modified graphite oxide (GO) in the presence of P3HT. Zhai and coworkers[20] showed that reduced graphene oxide (rGO) induced the formation of P3HT nanowires. Because of its large specific surface area and significant interface interactions, graphene is supposed to affect the crystallization behavior and microscopic structure of semicrystalline polymers.[21–23] Research on the crystallization behavior of P3HT/graphene nanocomposites can afford important information for optimizing the performance of organic photovoltaics based on graphene and P3HT; however, this remains quite lacking so far.

In this work, we report for the first time the effect of rGO on the nonisothermal crystallization behavior of P3HT. Several kinetics models were attempted to analyze the crystallization kinetics. The effective activation was calculated by the Kissinger equation. It is found that rGO remarkably increased the crystallization temperature and crystallinity of P3HT, but the crystallization rate of P3HT did not reveal obvious dependence on the rGO content.

EXPERIMENTAL

Materials and Preparation

Regioregular P3HT (M_n is 18,200, PDI is 1.7, H-T regioregularity is 98.5%) was synthesized following the Grignard metathesis method.[24] GO was prepared from natural graphite by a modified Hummers and Offeman method.[25] The resulting GO was dried at 65°C for 5 h and dried for 1 week in a desiccator before use. *N, N*-dimethylformamide (DMF), chloroform and 50% hydrazine hydrate were purchased from Shanghai Zhenxin Chemical Company (Shanghai, China), all chemicals were used

Applied Polymer SCIENCE

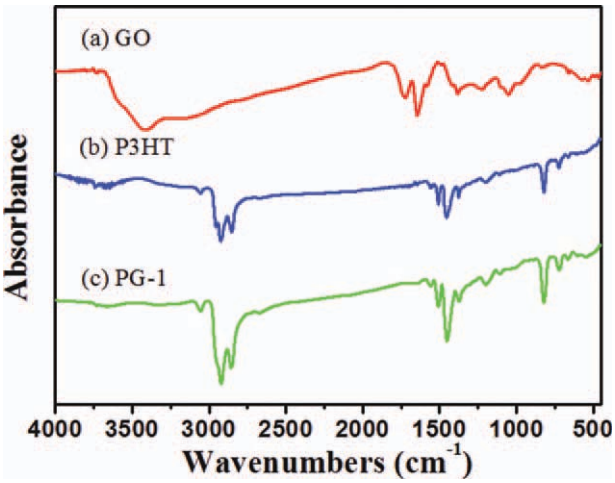

Figure 1. FTIR spectra of (a) GO, (b) P3HT, and (c) PG-1 nanocomposite. [Color figure can be viewed in the online issue, which is available at wileyonlinelibrary.com.]

as received. The P3HT/rGO nanocomposites were prepared through *in situ* reduction of GO in the presence of P3HT. Typically, the GO was first dispersed in DMF (0.5 mg mL^{-1}) by ultrasonication in an ultrasonic bath for 30 min. Then, the given volume of GO dispersion was mixed with the P3HT solution in chloroform (10 mL, 5 $mgmL^{-1}$) to yield the desired amount of GO (from 0.1–1 wt %), the composite solution was sonicated for another 30 min. A total of 50 μL hydrazine hydrate was added to the solution and then react for 24 h at 80°C. The resulting product was precipitated, filtered, and dried under vacuum at 70°C for 3 days. Nanocomposite samples PG-0.1, PG-0.2, PG-0.5, and PG-1 contained 0.1%, 0.2%, 0.5%, and 1% by weight of rGO in P3HT/rGO nanocomposites. For comparison, P3HT was also treated with hydrazine hydrate identical to the procedure used in preparing rGO/P3HT composites. All sample films for characterization were prepared by drop-casting the sample solutions (10 $mgmL^{-1}$ chloroform) on precleaned 22 × 22 mm^2 glass slides and drying in a vacuum oven preset at 60°C for 3 days.

Characterization

Fourier Transform Infrared Spectra. The Fourier transform infrared (FTIR) spectra of samples were recorded on a NEXUS 670 spectrometer in the range 4000–400 cm^{-1} with a resolution of 2 cm^{-1} using KBr pellets.

Atomic Force Microscope Image. For atomic force microscope (AFM) measurement, the graphene oxide dispersion was subjected to ultrasonication and then deposited onto a freshly cleaved mica surface. AFM characterization was performed with a Multimode Nano 4 instrument in tapping mode.

Wide-Angle X-Ray Diffraction. The as prepared films were used for wide-angle X-ray diffraction (WAXD) characterization. XRD data were collected using a PANalyticalX'Pert PRO X-ray diffractometer, operating at 40 kV and 40 mA, with Cu Kα radiation. Scans were made between 3° and 40°.

Transmission Electron Microscopy Observation. Transmission Electron Microscopy (TEM) image was taken with a Tecnai G2 F20 transmission electron microscope with an accelerating voltage of 100 kV. Sample film (PG-1) was encapsulated in epoxy matrixes and then sectioned into ultrathin sheets (~60 nm) by an ultra-microtome. These sheets were subsequently transferred onto holey carbon grids for TEM observation.

Differential Scanning Calorimetry Experiments. The nonisothermal crystallization behaviors were performed with a TA Q2000. The instrument was calibrated with standard indium, and all experiments were conducted under a nitrogen atmosphere. About 5 mg samples were used, all the samples were heated up to 260°C and kept for 10 min to remove previous history. Then, the samples were cooled to 20°C at cooling rates of 30, 20, 10, 5, and 2.5°C min^{-1}. The exothermic cures were recorded.

RESULTS AND DISCUSSION

Morphological and Structural Analysis

Graphene was prepared by exfoliation and reduction of GO. The FTIR spectra of GO, P3HT, and PG-1 nanocomposite are presented in Figure 1. GO contains a large amount of oxygen functional groups, the broad peak around 3418 cm^{-1} is attributed to the absorption of H-bonds, while other two peaks at 1725 and 1052 cm^{-1} arise from the vibrations of C=O and C—O, respectively.[26] For P3HT, the absorption band at 3054 cm^{-1} arises from the aromatic CH stretching vibration, and the bands at 2925 and 2854 cm^{-1} from the aliphatic CH stretching vibrations. The bands at 1508 and 1455 cm^{-1} are pertinent to the ring stretching, and 820 cm^{-1} to the out-of-plane vibration of aromatic C—H.[27] The characteristic peaks of P3HT are retained in PG-1 nanocomposite, while all peaks related to GO are absent. These results indicate that most of oxygen functional groups of GO have been removed by the reduction process, that is, GO is converted to rGO.[28]

Because GO possesses abundant polar functional groups such as hydroxyl, epoxide, and carboxyl, it is readily exfoliated into monolayers in water and polar solvents. Figure 2 presents the AFM image of the GO. It is seen that the majority of GO sheets are monolayer with an average thickness 0.59 nm and micron-sized lateral dimension. Figure 3 shows the TEM image of the

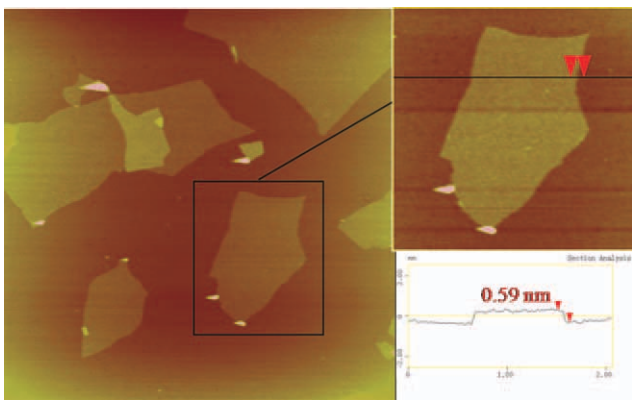

Figure 2. AFM image of GO deposited on a mica substrate. [Color figure can be viewed in the online issue, which is available at wileyonlinelibrary.com.]

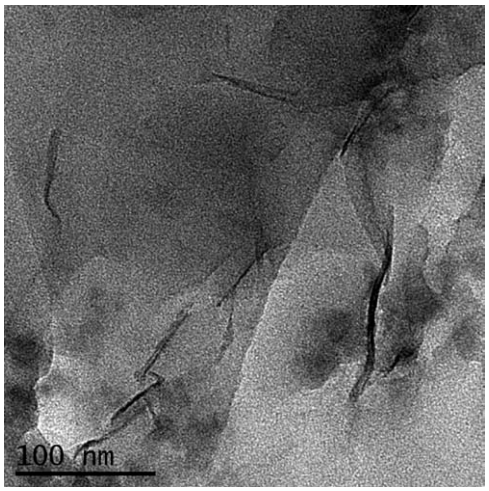

Figure 3. TEM image of PG-1 nanocomposite.

P3HT nanocomposite containing 1 wt % rGO (PG-1), where the rGO layers (dark lines), with a thickness < 4 nm and a length of ~100 nm, are found to be well dispersed in the P3HT matrix. There are no large rGO agglomerates observed, which can be attributed to the noncovalent P3HT-rGO interaction that prevents the aggregation in the *in situ* reduction process.[20]

The WAXD patterns of pristine graphite, GO, P3HT, and P3HT/rGO nanocomposites are shown in Figure 4. The strong peak at $2\theta = 26.5°$ from the pristine graphite disappeared in the pattern of GO. However, a new weak, broad peak $2\theta = 10.1°$ appeared in GO, implying an increased interlayer spacing from 0.34 to 0.86 nm after oxidation.[13,14] The diffraction peaks $2\theta = 5.6°$, 11.2°, and 16.6° correspond to the (100), (200), and (300) lattice plane of P3HT, respectively,[29] suggesting a 1.58 nm chain–chain interlayer distance. The diffraction peaks of P3HT in nanocomposites (PG-0.5 and PG-1) are similar to those in neat P3HT, indicating that the crystalline structure of P3HT did not change with the incorporation of rGO. The diffraction peaks of both graphite and GO are absent in the nanocomposites, suggesting that there are no rGO agglomerates in P3HT/rGO nanocomposites.

Nonisothermal Crystallization Results

The nonisothermal crystallization exotherms of P3HT and PG-0.5 (containing 0.5 wt % rGO) nanocomposite at different cooling rates are presented in Figure 5. The crystallization peak temperature (T_P), onset temperature (T_0), and crystallization enthalpy (ΔH_C) of P3HT and P3HT/rGO nanocomposites are listed in Table I. For these two samples, their T_0, T_P decrease and exothermal peaks become broader with increasing cooling rates, indicating that when the cooling rate was lowered, crystallization occurred at a higher temperature. The P3HT molecules can arrange themselves better at low cooling rates than at high cooling rates. This implies that smaller supercooling is required to initiate the crystallization of P3HT at lower cooling rates. In addition, it is noted that the T_0, T_P of the nanocomposites shift to higher temperatures compared with those of the neat P3HT, indicating that the rGO behaves as a nucleating agent for the

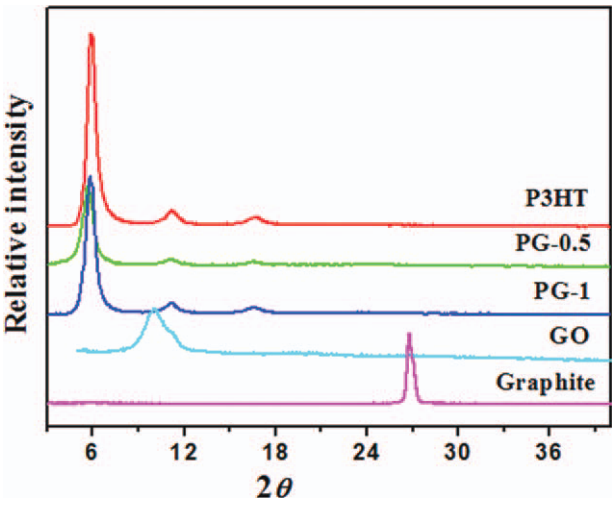

Figure 4. WAXD patterns of graphite, GO, P3HT, PG-0.5, and PG-1. [Color figure can be viewed in the online issue, which is available at wileyonlinelibrary.com.]

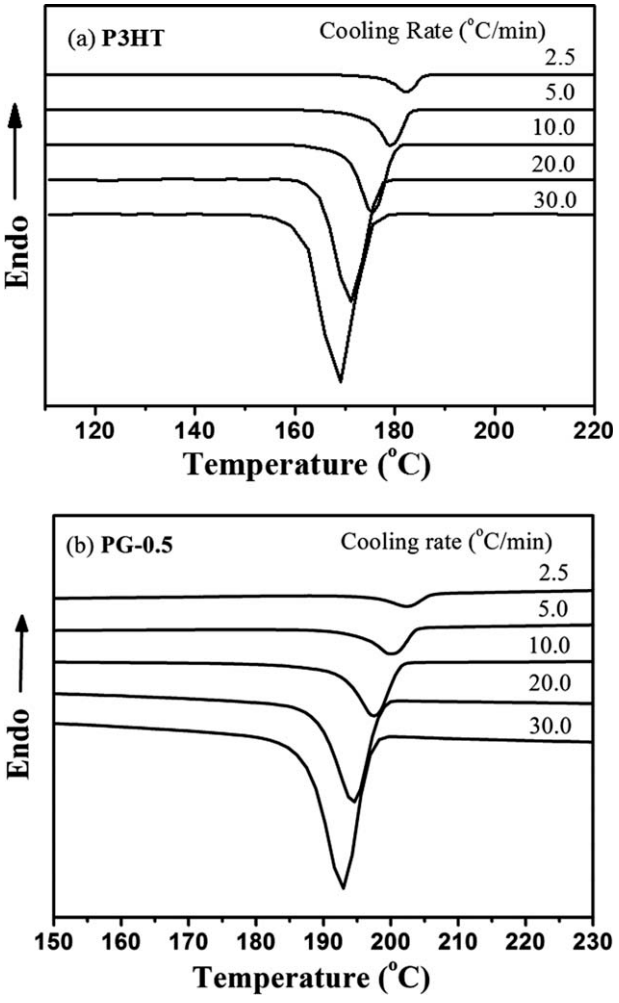

Figure 5. Differential scanning calorimetry exothermal curves of nonisothermal crystallization with different cooling rates for (a) P3HT and (b) PG-0.5 nanocomposite.

Table I. Nonisothermal Crystallization Kinetic Parameters for All Samples

Sample	φ (°C min^{-1})	T_0 (°C)	T_P (°C)	$t_{1/2}$	ΔH_C (J g^{-1})	n	K_C
P3HT	2.5	187.9	182.47	3.02	6.37	3.64	0.2042
	5	185.9	179.39	1.26	8.76	3.91	0.6567
	10	182.1	175.09	0.72	7.58	3.24	1.0065
	20	179.9	171.41	0.46	8.09	3.66	1.1325
	30	178.8	168.95	0.35	6.98	2.44	1.1079
PG-0.1	2.5	206	197.47	4.19	11.75	4.07	0.0925
	5	202.9	194.13	2.08	13.29	3.71	0.5666
	10	201.8	191.22	1.17	13.49	4.69	0.9301
	20	198.8	189.40	0.57	10.84	3.96	1.1043
	30	194.7	187.49	0.50	12.27	5.71	1.1395
PG-0.2	2.5	209.5	201.58	3.62	13.51	4.50	0.0880
	5	205.9	198.82	1.59	14.56	3.80	0.6632
	10	202.9	195.89	0.76	14.43	3.29	1.0581
	20	199.3	193.99	0.44	13.71	3.29	1.1216
	30	198.4	190.83	0.36	13.36	4.02	1.1325
PG-0.5	2.5	212.3	202.35	4.44	13.63	5.22	0.0371
	5	208	199.92	1.81	14.10	5.17	0.5066
	10	203.4	197.54	0.68	14.46	3.49	1.1019
	20	200.8	194.60	0.36	12.58	3.48	1.1732
	30	199.6	192.95	0.25	12.91	3.51	1.1613
PG-1	2.5	202.7	194.81	4.14	9.945	3.03	0.1616
	5	201.2	191.17	2.49	10.35	3.66	0.4898
	10	199.4	187.65	1.45	10.92	4.31	0.8379
	20	194	184.65	0.62	9.975	3.05	1.0611
	30	191.4	180.32	0.44	9.163	3.62	2.5539

crystallization of P3HT. Furthermore, among the four nanocomposites, the T_P of PG-0.5 nanocomposite reveals the highest value. This can be attributed to two factors. First, the number of nucleation sites increases with increasing rGO contents, which is favorable for the crystallization of P3HT. Second, further addition of rGO introduces more steric hindrance, limiting the mobility of P3HT chains. In this regard, Hua et al.[21] have showed a similar trend. When the content of GO in poly(ε-caprolactone)/GO (PCL-GO) composites increased from 1.5 to 6 wt %, GO was found to limit the mobility of PCL chains, leading to a lowered T_P in PCL-GO (6 wt %). On the other hand, the ΔH_C of P3HT/rGO nanocomposites are higher than that of the neat P3HT at a given cooling rate, suggesting that rGO enhances the total crystallinity of P3HT in the nanocomposites. Similar phenomenon can also be seen in P3HT-single walled carbon nanotube systems.[30]

Nucleation activity (ε) can be defined as the ratio between the work of three-dimensional nucleation with and without a foreign substrate. If a foreign filler is extremely active for nucleation, the value of ε approaches 0, while ε approaches 1 for an absolutely inert filler. Dobreva and Gutzow[31,32] proposed a simple method to determine the nucleation activity of the foreign filler, that is, the nucleation activity can be calculated by,

$$\varepsilon = \frac{B*}{B} \tag{1}$$

where B and B^* represent parameters in homogenous and heterogeneous nucleation. It is determined experimentally from the slope of following equation,

$$\log \varphi = A - \frac{B}{\Delta T_P^2} \tag{2}$$

where φ is the cooling rate, A is a constant, and ΔT_P is the supercooling ($T_m - T_P$).

The plots of log φ versus $1/\Delta T_P^2$ for P3HT and P3HT/rGO nanocomposites are presented in Figure 6, and the values of B for P3HT is 4.7137, while B^* for PG-0.1, PG-0.2, PG-0.5, and PG-1 are 3.0594, 2.9546, 2.8955, and 3.2245, respectively. The values of nucleation activity ε for PG-0.1, PG-0.2, PG-0.5, and PG-1 are 0.649, 0.6268, 0.6143, and 0.6841, respectively. These values less than 1 indicate that rGO acts as effective nucleating agent in P3HT/rGO nanocomposites. The value of ε for PG-0.5 is the lowest, indicating the strongest nucleation effect appeared at 0.5 wt % rGO content, which is consistent with the highest T_P of PG-0.5.

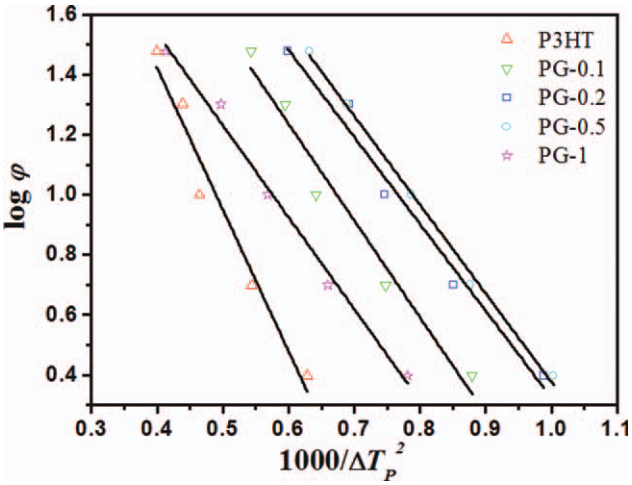

Figure 6. Plots of log φ versus $1/\Delta T_P^2$ for P3HT and P3HT/rGO nanocomposites. [Color figure can be viewed in the online issue, which is available at wileyonlinelibrary.com.]

For a nonisothermal crystallization process, the relative crystallinity, X_T, as a function of crystallization temperature, can be defined as follows:

$$X_T = \frac{\int_{T_0}^{T} (dH/dT)dT}{\int_{T_0}^{T_\infty} (dH/dT)dT} \quad (3)$$

where T_0 and T_∞ represent the initial and end crystallization temperature, respectively; dH/dT is the heat flow rate. In the nonisothermal crystallization, the time t and temperature T have the following relation:

$$t = \frac{T_0 - T}{\varphi} \quad (4)$$

Figure 7 shows the changes of relative crystallinity as a function of temperature and time for P3HT and PG-0.5 nanocomposite. The values of crystallization half-time $t_{1/2}$ of all samples are also listed in Table I. Compared with P3HT, the $t_{1/2}$ values exhibit little variation after the addition of rGO. This seems to be different from the results reported in the literature. In a previous report, Zhai and coworkers[20] showed that rGO greatly accelerated the quasi-isothermal solution crystallization of P3HT. It is supposed that the discrepancy might result from different crystallization conditions. The π-π interaction between P3HT and rGO has contrary influences on P3HT crystallization. On the one hand, the π-π interaction can induce P3HT chains orientation along the graphitic domains of rGO, exhibiting a nucleation effect, which prompts the crystallization of P3HT. On the other hand, the π-π interaction restricts the migration and diffusion of P3HT chains, and thus, suppresses the crystallization of P3HT. For a solution crystallization process, the diffusion of P3HT chains may suffer from relatively weak influence, particularly for those crystallization processes in dilute solutions.

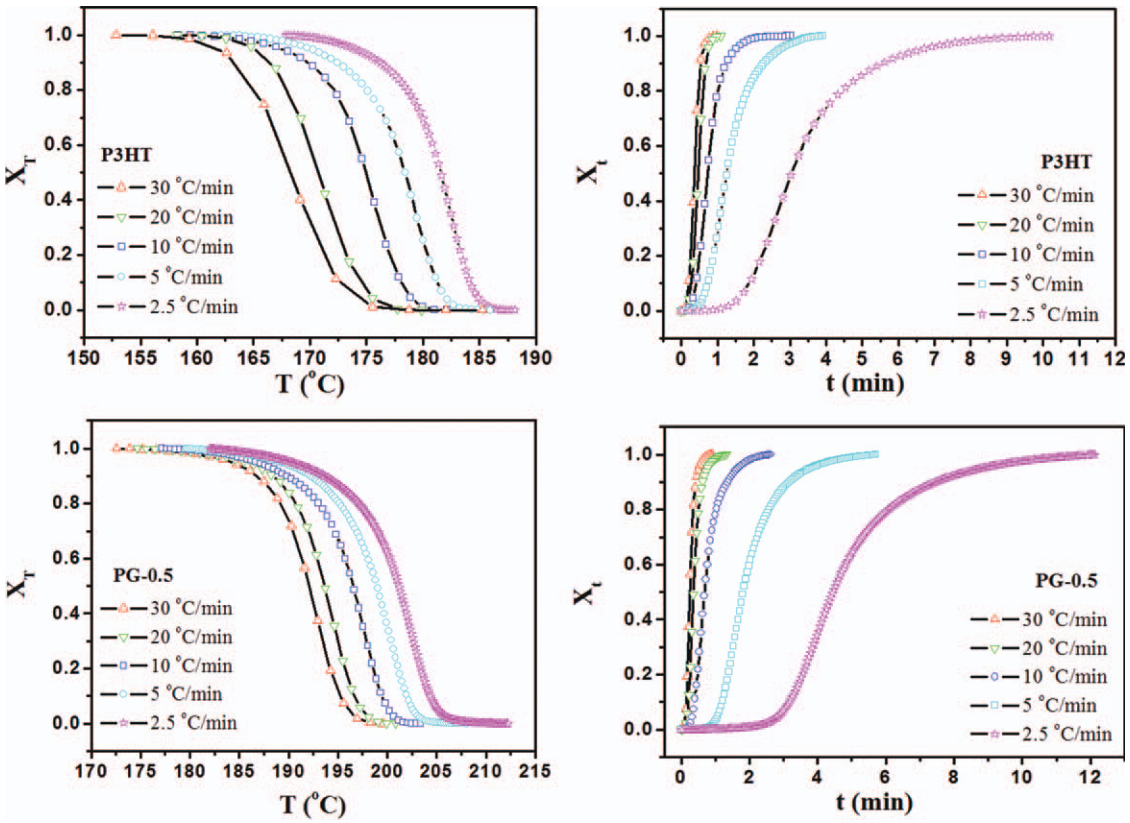

Figure 7. Plots of relative crystallinity as a function of temperature T (left) and time t (right) at different cooling rates for P3HT and PG-0.5 nanocomposite. [Color figure can be viewed in the online issue, which is available at wileyonlinelibrary.com.]

Applied Polymer SCIENCE

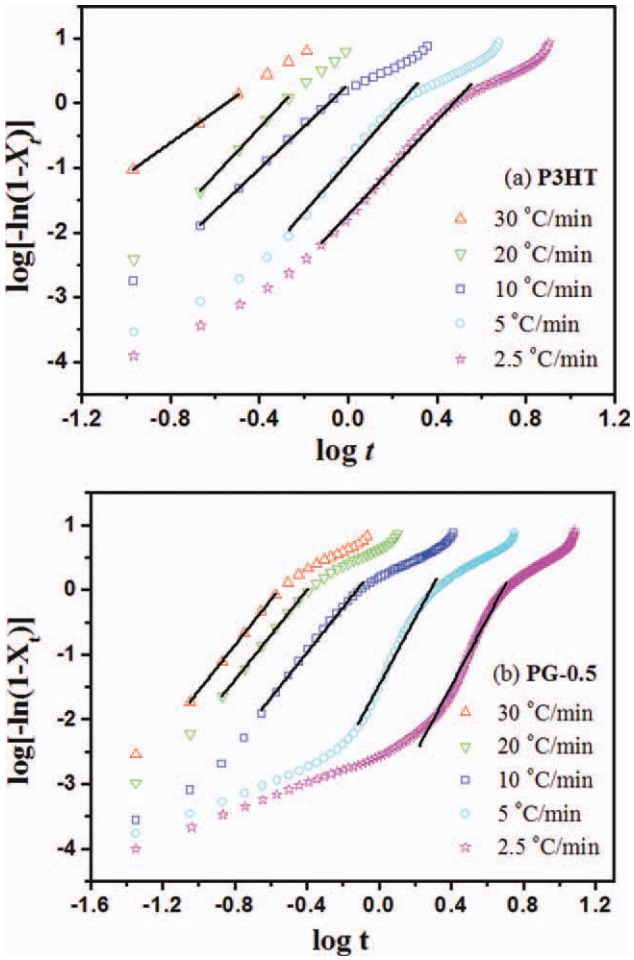

Figure 8. Plots of log[−ln(1 − X_t)] versus log t for (a) P3HT and (b) PG-0.5 nanocomposite. [Color figure can be viewed in the online issue, which is available at wileyonlinelibrary.com.]

Consequently, the nucleation effect would be dominant in this case. However, for a melt crystallization process, the restriction effect will become remarkable, which will greatly impair the contribution of the nucleation effect to the total crystallization rate.

Kinetic Analysis Based on the Avrami Model

The Avrami model for the analysis of the nonisothermal crystallization kinetics of P3HT and P3HT/rGO nanocomposites can be expressed as follows[33,34]:

$$1 - X_t = \exp(-Kt^n) \tag{5}$$

or

$$\log[-\ln(1 - X_t)] = \log K + n \log t \tag{6}$$

where n is the Avrami exponent depending on the nucleation and growth process of crystallization, and K is the temperature-dependent rate constant. Considering the constant cooling rate φ in the nonisothermal process, Jeziorny[35] gave the corrected form of K as follows:

$$\log K_C = \frac{\log K}{\varphi} \tag{7}$$

Figure 8 presents the plots of log[−ln(1 − X_t)] versus log t for P3HT and P3HT/rGO nanocomposites. The values of the Avrami exponent n and the rate constant K or K_C can be obtained from the slope and intercept of linear region.[36] Because the middle portion of the curves occupied the range 0.3%–63% of the crystallization process, the n, K, and K_C values are adopted from the middle portion of these curves and summarized in Table I. The values of n ranged from 2.44 to 3.91 for P3HT and from 3.03 to 5.71 for nanocomposites. The values of n are nonintegers, and some of them are even higher than 4, suggesting a complicated crystallization mechanism. The values of K_C associated with nucleation and growth rates are comparable for P3HT and nanocomposites. They suggest that the incorporation of rGO does not significantly change the nonisothermal crystallization rates of P3HT, due to the competition between the nucleation and restriction effects.

Kinetic Analysis Based on the Ozawa Model

Considering the nonisothermal crystallization is a cooling rate dependent process, Ozawa[37] presented an extended Avrami model,

$$1 - X_T = \exp[-Z(T)/\varphi^m] \tag{8}$$

where $Z(T)$ is the crystallization rate constant and m is the Ozawa exponent. Equation (8) can be rearranged in a logarithmic form:

$$\log[-\ln(1 - X_T)] = \log Z(T) - m \log \varphi \tag{9}$$

The plots of log[−ln(1 − X_T)] versus log φ for P3HT and PG-0.5 nanocomposite are shown in Figure 9. If the Ozawa model can correctly describe the nonisothermal crystallization kinetics, the plots would give a series of parallel straight lines, $Z(T)$ and m can thus be determined from the intercept and the slope, respectively. However, no such straight lines for P3HT and PG-0.5 nanocomposite are obtained, as shown in Figure 9. This means that the Ozawa model fails to effectively describe the nonisothermal crystallization of P3HT and nanocomposites. Similar results were also observed on analyzing the nonisothermal crystallization of poly(3-dodecylthiophene).[9] The reason may result from the secondary crystallization occurred in melt crystallization processes; the latter was not considered in the Ozawa model.

Kinetic Analysis Based on the Combined Avrami and Ozawa Model

In view of the fact that both the Avrami and Ozawa models cannot be used to effectively describe nonisothermal crystallization of polymer melts, Mo and coworkers[38] developed a new kinetic model by combing the Avrami and Ozawa models:

$$\log K + n \log t = \log Z(T) - m \log \varphi \tag{10}$$

$$\log \varphi = \log F(T) - \alpha \log t \tag{11}$$

where parameter $F(T) = [Z(T)/K]^{1/m}$ refers to the value of the cooling rate when the system reaches a certain degree of

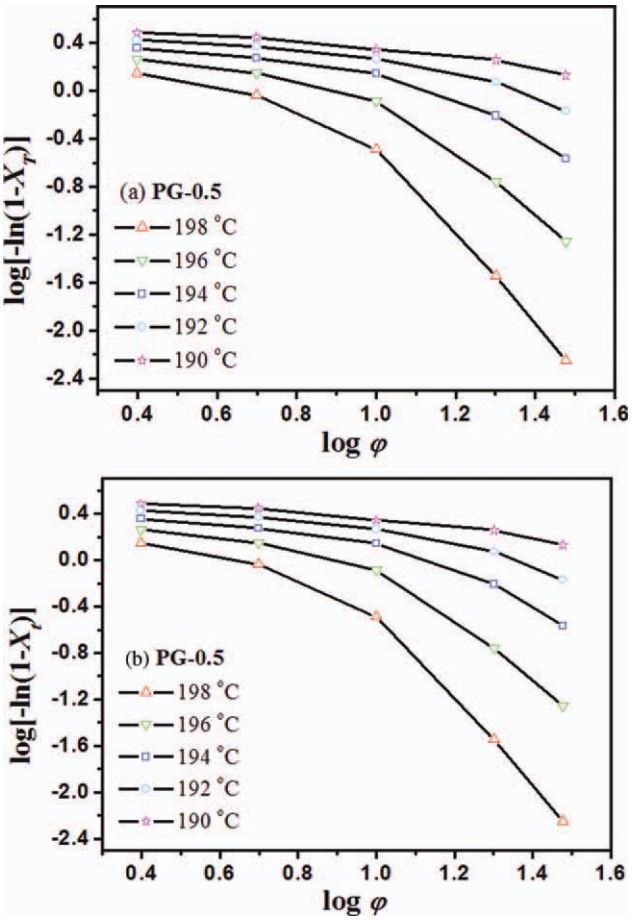

Figure 9. Ozawa plots of log[−ln(1 − X_T)] versus log φ at indicated temperatures for (a) P3HT and (b) PG-0.5 nanocomposite. [Color figure can be viewed in the online issue, which is available at wileyonlinelibrary.com.]

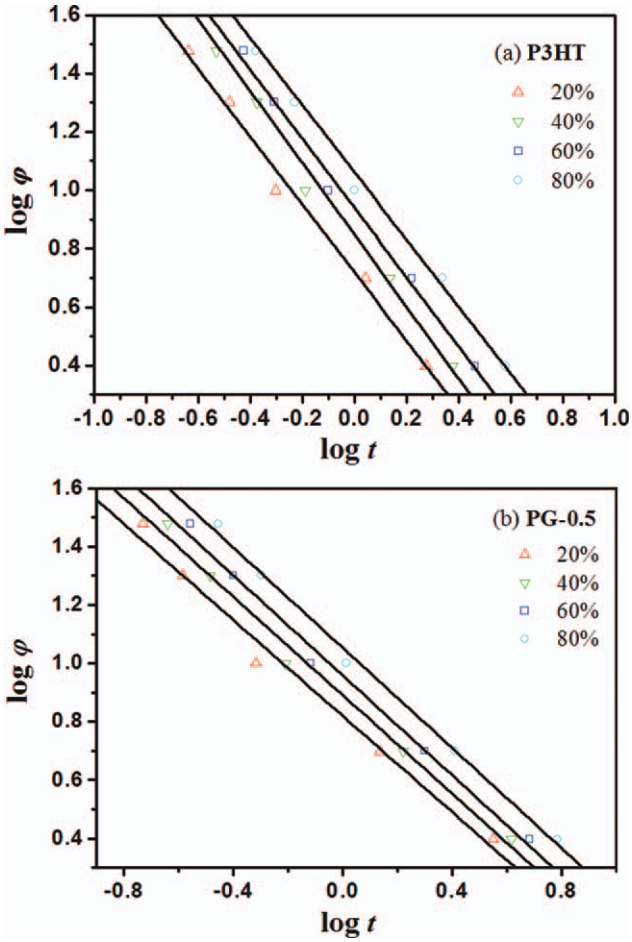

Figure 10. Plots of log φ versus log t for the nonisothermal crystallization of (a) P3HT and (b) PG-0.5 nanocomposite. [Color figure can be viewed in the online issue, which is available at wileyonlinelibrary.com.]

crystallinity in the unit time. $F(T)$ has a definite physical implication, that is, the higher the value of $F(T)$, the slower the crystallization rates. α is the ratio of the Avrami exponent n to the Ozawa exponent m. Plots of log φ versus log t at different degree of crystallinity are shown in Figure 10. The good linearity of the plots suggests the validity of this improved model in describing the nonisothermal crystallization of P3HT and P3HT/rGO nanocomposites. The parameter $F(T)$ and α are listed in Table II. It can be seen that α values reveal a very limited change. The value of $F(T)$ increased with increasing relative crystallinities for all samples. In addition, at a certain crystallinity, $F(T)$ of nanocomposites decreases first with increasing rGO contents from 0.1% to 0.2% but increases on further increasing rGO contents in P3HT. This suggests that a large amount of rGO lowers the crystallization rate. As aforementioned, rGO significantly suppresses the chain diffusion of P3HT due to the strong π-π interaction between P3HT and rGO. Similar applications of the improved model have been conducted successfully in analyzing nonisothermal kinetics of poly(3-dodecylthiophene),[9] PA6/GO nanocomposites.[22,23]

Crystallization Activation Energy

For the nonisothermal crystallization, the activation energy can be derived from the combination of crystallization peak temperature (T_P) and cooling rate (φ) by the Kissinger[39] equation:

$$\frac{d(\ln(\varphi/T_P^2))}{d(1/T_P)} = -\frac{\Delta E}{R} \tag{12}$$

Table II. Values of α and $F(T)$ for P3HT and Nanocomposites

X_t (%)		20	40	60	80
P3HT	α	1.1633	1.2304	1.1841	1.1498
	$F(T)$	5.2293	7.0432	8.6974	11.5205
PG-0.1	α	1.0717	1.0624	1.0550	1.0228
	$F(T)$	7.8071	10.1062	12.6870	16.4756
PG-0.2	α	0.9428	0.9657	0.9881	0.9925
	$F(T)$	5.9605	7.5071	9.2638	11.9396
PG-0.5	α	0.8225	0.8430	0.8559	0.8580
	$F(T)$	6.5989	7.7825	9.0985	11.3058
PG-1	α	1.0908	1.0880	1.0963	1.0798
	$F(T)$	8.4202	11.2933	14.9018	20.4527

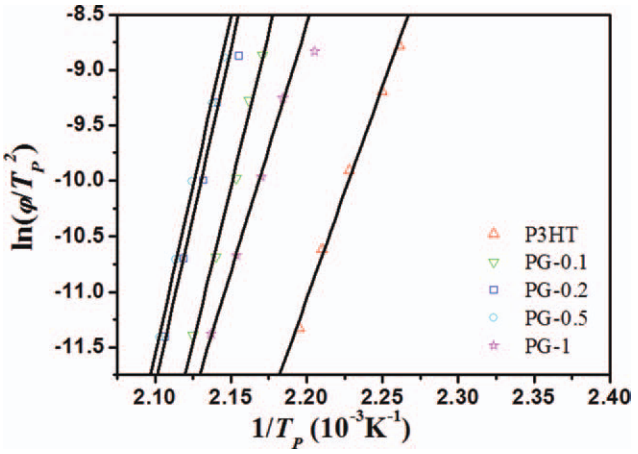

Figure 11. Plots of $\ln(\varphi/T_P^2)$ versus $1/T_P$ for P3HT and P3HT/rGO nanocomposites. [Color figure can be viewed in the online issue, which is available at wileyonlinelibrary.com.]

Table III. The ΔE Values of P3HT and Nanocomposites

Sample	P3HT	PG-0.1	PG-0.2	PG-0.5	PG-1
ΔE (kJ mol^{-1})	319.01	463.28	501.49	506.5	370.28

where R is the gas constant and ΔE is the activation energy. ΔE, composed of the transport activation energy ΔE^* and the nucleation activation energy ΔF, is related to the energy barrier for a polymer segments moving toward the growing front of a crystal. Figure 11 shows the plots of $\ln(\varphi/T_P^2)$ versus $1/T_P$ for P3HT and P3HT/rGO nanocomposites. The values of the activation energy are listed in Table III. The values of ΔE remarkably increased for the PG-0.1, PG-0.2 nanocomposites, and slightly increased for the PG-0.5 nanocomposite. However, the value of ΔE is smaller in PG-1 nanocomposite than other nanocomposites. This trend is similar to the experimental observation of Nylon/f-MWCNT nanocomposites reported by Chen and Wu.[40] The addition of 0.1–1 wt % rGO in the P3HT suppresses the motion of P3HT chains, and meanwhile, the heterogeneous nucleation effect is not sufficient to offset the influence of the restriction effect so that the ΔE of the nanocomposite is higher than the neat P3HT. For the nanocomposite loaded with 1 wt % rGO, due to the presence of more heterogeneous nucleation sites, resulting in a lower ΔE relative to other nanocomposites.

CONCLUSION

The P3HT/rGO nanocomposites with different rGO contents were prepared via *in situ* reduction of GO in the presence of P3HT. Several kinetics models were used to analyze the nonisothermal crystallization behavior of P3HT and nanocomposites. The modified Avrami and Ozawa models failed to effectively describe the nonisothermal crystallization behavior of P3HT and nanocomposites. In contrast, the combined Avrami-Ozawa model proposed by Mo and coworkers can be used to describe their crystallization process. Compared with the neat P3HT, the crystallization peak temperature and crystallinity of P3HT in nanocomposites dramatically increased, although the change in the crystallization half-time is slight. The activation energy determined by the Kissinger model first increases and then decreases. This would be attributed to the restriction effect of rGO to P3HT and the reduced mobility of polymer chains. Further increasing the GO content in P3HT introduced more heterogeneous nucleation sites and thus reduced the activation energy of P3HT in nanocomposites.

ACKNOWLEDGMENTS

The authors are grateful to Lianhua Long (Fudan Univ.) for providing P3HT sample. This work was supported by The National High Technology Research and Development Program of China (Grant No. 2008AA032102), NSF of China (Grant No. 50573014, 50773012, and 51173027), and Shanghai Nanotechnology Program (Grant No. 1052nm00400).

REFERENCES

1. Sirringhaus, H.; Brown, P. J.; Friend, R. H.; Nielsen, M. M.; Bechgaard, K.; Langeveld-Voss, B. M. W.; Spiering, A. J. H.; Janssen, R. A. J.; Meijer, E. W.; Herwig, P.; de Leeuw, D. M. *Nature* **1999,** *401*, 685.
2. Kim, Y.; Cook, S.; Tuladhar, S. M.; Choulis, S. A.; Nelson, J.; Durrant, J. R.; Bradley, D. D. C.; Giles, M.; McCulloch, I.; Ha, C.; Ree, M. *Nat. Mater.* **2006,** *5*, 197.
3. Zhao, Y.; Guo, X. Y.; Xie, Z. Y.; Qu, Y.; Geng, Y. H.; Wang, L. X. *J. Appl. Polym. Sci.* **2009,** *111*, 1799.
4. Brinkmann, M.; Wittmann, J. *Adv. Mater.* **2006,** *18*, 860.
5. Zen, A.; Saphiannikova, M.; Neher, D.; Grenzer, J.; Grigorian, S.; Pietsch, U.; Asawapirom, U.; Janietz, S.; Scherf, U.; Lieberwirth, I.; Wegner, G. *Macromolecules* **2006,** *39*, 2162.
6. Causin, V.; Marega, C.; Marigo, A.; Valentini, L.; Kenny, J. M. *Macromolecules* **2005,** *38*, 409.
7. Malik, S.; Nandi, A. K. *J. Polym. Sci. Part B: Polym. Phys.* **2002,** *40*, 2073.
8. Pal, S.; Nandi, A. K. *J. Appl. Polym. Sci.* **2006,** *101*, 3811.
9. Liu, S. L.; Chung, T. S. *Polymer* **2000,** *41*, 2781.
10. Lilliu, S.; Agostinelli, T.; Pires, E.; Hampton, M.; Nelson, J.; Macdonald, J. M. *Macromolecules* **2011,** *44*, 2725.
11. Swinnen, A.; Haeldermans, I.; Vanlaeke, P.; D'Haen, J.; Poortmans, J.; D'Olieslaeger, M.; Manca, J. V. *Eur. Phys. J. Appl. Phys.* **2007,** *36*, 251.
12. Geim, A. K. *Science* **2009,** *324*, 1530.
13. Fang, M.; Wang, K. G.; Lu, H. B.; Yang, Y. L.; Nutt, S. *J. Mater. Chem.* **2009,** *19*, 7098.
14. Chen, Z. X.; Lu, H. B. *J. Mater. Chem.* **2012.** DOI: 10.1039/c2jm30517h.
15. Stankovich, S.; Dikin, D. A.; Dommett, G. H. B.; Kohlhaas, K. M.; Zimney, E. J.; Stach, E. A.; Piner, R. D.; Nguyen, S. T.; Ruoff, R. S. *Nature* **2006,** *442*, 282.
16. Ramanathan, T.; Abdala, A. A.; Stankovich, S.; Dikin, D. A.; Herrera-Alonso, M.; Piner, R. D.; Adamson, D. H.; Schniepp, H. C.; Chen, X.; Ruoff, R. S.; Nguyen, S. T.; Aksay, I. A.; Prud'Homme, R. K.; Brinson, L. C. *Nat. Nanotechnol.* **2008,** *3*, 327.

17. Liu, Z. F.; Liu, Q.; Huang, Y.; Ma, Y. F.; Yin, S. G.; Zhang, X. Y.; Sun, W.; Chen, Y. S. *Adv. Mater.* **2008,** *20*, 3924.
18. Liu, Q.; Liu, Z. F.; Zhang, X. Y.; Yang, L. Y.; Zhang, N.; Pan, G. L.; Yin, S. G.; Chen, Y. S.; Wei, J. *Adv. Funct. Mater.* **2009,** *19*, 894.
19. Yang, Z. L.; Shi, X. J.; Yuan, J. J.; Pu, H. T.; Liu, Y. S. *Appl. Surf. Sci.* **2010,** *257*, 138.
20. Chunder, A.; Liu, J. H.; Zhai, L. *Macromol. Rapid Commun.* **2010,** *31*, 380.
21. Hua, L.; Kai, W. H.; Inoue, Y. *J. Appl. Polym. Sci.* **2007,** *106*, 4225.
22. Liu, Y.; Yang, G. S. *Thermochim. Acta* **2010,** *500*, 13.
23. Zhang, F.; Peng, X. C.; Yan, W. B.; Peng, Z. Y.; Shen, Y. Q. *J. Polym. Sci. Part B: Polym. Phys.* **2011,** *49*, 1381.
24. Loewe, R. S.; Khersonsky, S. M.; McCullough, R. D. *Adv. Mater.* **1999,** *11*, 250.
25. Hummers, W. S.; Offeman, R. E. *J. Am. Chem. Soc.* **1958,** *80*, 1339.
26. Heo, C.; Moon, H.-G.; Yoon, C. S.; Chang J.-H. *J. Appl. Polym. Sci.* **2012,** *124*, 4663.
27. Kuila, B. K.; Nandi, A. K. *Macromolecules* **2004,** *37*, 8577.
28. Chang, Y.-W.; Yu, S.-W.; Liu, C.-H.; Tsing, R. C.-C. *J. Nanosci. Nanotechnol.* **2010,** *10*, 6520.
29. Hugger, S.; Thomann, R.; Heinzel, T.; Thurn-Albrecht, T. *Colloid Polym. Sci.* **2004,** *282*, 932.
30. Geng, J. X.; Zeng, T. Y. *J. Am. Chem. Soc.* **2006,** *128*, 16827.
31. Dobreva, A.; Gutzow, I. *J. Non-Cryst. Solids* **1993,** *162*, 1.
32. Dobreva, A.; Gutzow, I. *J. Non-Cryst. Solids* **1993,** *162*, 13.
33. Avrami, M. *J. Chem. Phys.* **1940,** *8*, 212.
34. Avrami, M. *J. Chem. Phys.* **1941,** *9*, 177.
35. Jeziorny, A. *Polymer* **1978,** *19*, 1142.
36. Weng, W. G.; Chen, G. H.; Wu, D. J. *Polymer* **2003,** *44*, 8119.
37. Ozawa, T. *Polymer* **1971,** *12*, 150.
38. Liu, T. X.; Mo, Z. S.; Zhang, H. F. *J. Appl. Polym. Sci.* **1998,** *67*, 815.
39. Kissinger, H. E. *J. Res. Natl. Bur. Stand.* **1956,** *57*, 217.
40. Chen, E.-C.; Wu, T.- M. *J. Polym. Sci. Part B: Polym. Phys.* **2008,** *46*, 158.